NUMERICAL INVESTIGATION OF ALUMINUM BURNING BEHIND BLAST WAVES

F. Togashi[1], J. D. Baum[1], R. Lohner[2], O. Soto[1], and A. Amini[3]

[1]Science Application International Corporation, 1710 SAIC Dr., MS 2-6-9, McLean, VA 22102, USA; [2]George Mason University, Dept. of Computational and Data Science, College of Science, MS 6A2, Fairfax, VA 22030, USA; [3]Defense Thread Reduction Agency, Fort Belvoir, VA 22060, USA

ABSTRACT

Energy release by aluminum burning behind the blast wave front produced by heavily aluminized explosives was investigated. An aluminum evaporation/reaction model within the multi-phase flow was applied. The modeled HE includes a significant percentage of aluminum particles, whose long-time afterburning and energy release must be considered.

As a first step in the overall 3-D comprehensive methodology development, the evaporation of small aluminum particles, with 5, 50, and 500μm diameter, was investigated in a 1-D code. The aluminum particles can react with oxygen, water, and carbon dioxide. The resulting pressure profiles are different from those obtained for the no-reaction case or using a one-reaction which only consider the reaction with oxygen. Finally this aluminum burning model was incorporated into our in-house 3-D code, FEFLO.

HEADING

Aluminum particles are often mixed into explosives and solid propellants to increase their energy release. The Aluminum particles are capable of burning behind the detonation front and their combustion time under such high pressure/temperature conditions is significantly longer than detonation time. If such heavily aluminized HEs/propellants are cased, the physical mechanisms are even more complex. The flow environment is significantly different from bare charge detonation and afterburn. As long as the case is intact, no external air (oxygen) is available, so most of the aluminum particles cannot burn other than in anaerobic reaction, which is fairly limited for explosives with high loading of aluminum particles. Hence, establishing a valid energy release model of aluminum burning behind the detonation front (afterburning) is required for the accurate modeling of cased aluminized explosives. Developing an accurate numerical Al burnig model is not trivial as the HE chemical reactions are very complicated, and the aluminum reaction controlling mechanisms behind the detonation front have not been yet fully established.

Kim *et al*. and Balakrishnan *et al*. have reported the numerical simulation of the aluminum afterburning behind TNT detonations [1, 2]. They applied the Khasainov's empirical quasi-steady law [3] for aluminum evaporation in a multi-phase flow and simple chemical reaction model using infinite chemical reaction rates [4, 5] to the afterburning behind the blast wave. Nobel-Abel EOS [6] was applied to the main computation of the blast wave propagation and TNT ($C_7H_5N_3O_6$) was assumed to decompose to 4 species such as N_2, H_2O, CO, and C as follows: $C_7H_5N_2O_6 \rightarrow 1.5N_2 + 2.5H_2O + 3.5CO + 3.5C$ [7]. However, practical explosives/propellants are often composites of HEs, oxidizers, and binders.

Report Documentation Page

Form Approved
OMB No. 0704-0188

1. REPORT DATE	2. REPORT TYPE	3. DATES COVERED
OCT 2010	**N/A**	**-**

4. TITLE AND SUBTITLE	5a. CONTRACT NUMBER
Numerical Investigation Ofaluminum Burning Behind Blast Waves	5b. GRANT NUMBER
	5c. PROGRAM ELEMENT NUMBER
6. AUTHOR(S)	5d. PROJECT NUMBER
	5e. TASK NUMBER
	5f. WORK UNIT NUMBER
7. PERFORMING ORGANIZATION NAME(S) AND ADDRESS(ES)	8. PERFORMING ORGANIZATION REPORT NUMBER
Science Application International Corporation, 1710 SAIC Dr., MS 2-6-9, McLean, VA 22102	
9. SPONSORING/MONITORING AGENCY NAME(S) AND ADDRESS(ES)	10. SPONSOR/MONITOR'S ACRONYM(S)
	11. SPONSOR/MONITOR'S REPORT NUMBER(S)

12. DISTRIBUTION/AVAILABILITY STATEMENT

Approved for public release, distribution unlimited

13. SUPPLEMENTARY NOTES

See also ADA550809. Military Aspects of Blast and Shock (MABS 21) Conference proceedings held on October 3-8, 2010. Approved for public release; U.S. Government or Federal Purpose Rights License, The original document contains color images.

14. ABSTRACT

Energy release by aluminum burning behind the blast wave front produced by heavily aluminized explosives was investigated. An aluminum evaporation/reaction model within the multi-phase flow was applied. The modeled HE includes a significant percentage of aluminum particles, whose long-time afterburning and energy release must be considered. As a first step in the overall 3-D comprehensive methodology development, the evaporation of small aluminum particles, with 5, 50, and 500ìm diameter, was investigated in a 1-D code. The aluminum particles can react with oxygen, water, and carbon dioxide. The resulting pressure profiles are different from those obtained for the no-reaction case or using a one-reaction which only consider the reaction with oxygen. Finally this aluminum burning model was incorporated into our in-house 3-D code, FEFLO.

15. SUBJECT TERMS

16. SECURITY CLASSIFICATION OF:			17. LIMITATION OF ABSTRACT	18. NUMBER OF PAGES	19a. NAME OF RESPONSIBLE PERSON
a. REPORT	b. ABSTRACT	c. THIS PAGE			
unclassified	**unclassified**	**unclassified**	**SAR**	**14**	

The objective in this study is to develop a numerical model of aluminum particle burning behind the blast wave (afterburning) of heavily aluminized explosives and to establish a reasonable numerical model without resorting to expensive CPU calculations.

FLOW SOLVER AND CHEMICAL REACTION MODELING

The governing equations are as follows:

$$\frac{\partial \mathbf{Q}}{\partial t}+\frac{\partial \mathbf{E}}{\partial x}+\frac{\partial \mathbf{F}}{\partial y}+\frac{\partial \mathbf{G}}{\partial z}=S_1+S_2+S_3 \qquad (1)$$

$$Q=\begin{bmatrix}\rho_{gk}\\ \rho_g\\ \rho_g u_g\\ \rho_g v_g\\ \rho_g w_g\\ e_g\\ \phi_s\rho_s\\ \phi_s\rho_s u_s\\ \phi_s\rho_s v_s\\ \phi_s\rho_s w_s\\ \phi_s\rho_s E_s\\ N_p\end{bmatrix}, E=\begin{bmatrix}\rho_{gk}u_g\\ \rho_g u_g\\ \rho_g u_g^{\,2}+P\\ \rho_g u_g v_g\\ \rho_g u_g w_g\\ (e_g+P)u_g\\ \phi_s\rho_s u_s\\ \phi_s\rho_s u^2{}_s\\ \phi_s\rho_s v_s u_s\\ \phi_s\rho_s w_s u_s\\ \phi_s\rho_s E_s u_s\\ N_p u_s\end{bmatrix}, F=\begin{bmatrix}\rho_{gk}v_g\\ \rho_g v_g\\ \rho_g v_g u_g\\ \rho_g v_g^{\,2}+P\\ \rho_g v_g w_g\\ (e_g+P)v_g\\ \phi_s\rho_s v_s\\ \phi_s\rho_s u_s v_s\\ \phi_s\rho_s v^2{}_s\\ \phi_s\rho_s w_s v_s\\ \phi_s\rho_s E_s v_s\\ N_p v_s\end{bmatrix}, G=\begin{bmatrix}\rho_{gk}w_g\\ \rho_g w_g\\ \rho_g w_g u_g\\ \rho_g w_g v_g\\ \rho_g w_g^{\,2}+P\\ (e_g+P)w_g\\ \phi_s\rho_s w_s\\ \phi_s\rho_s u_s w_s\\ \phi_s\rho_s v_s w_s\\ \phi_s\rho_s w^2{}_s\\ \phi_s\rho_s E_s w_s\\ N_p w_s\end{bmatrix},$$

$$S_1 = \begin{bmatrix} \frac{1}{1-\phi_s}\xi_k \Delta c(1-\frac{\rho_g}{\rho_s}) + \dot{\omega}_k \\ \frac{1}{1-\phi_s}\Delta c(1-\frac{\rho_g}{\rho_s}) \\ \frac{1}{1-\phi_s}\Delta c(u_s - u_g\frac{\rho_g}{\rho_s}) \\ \frac{1}{1-\phi_s}\Delta c(v_s - v_g\frac{\rho_g}{\rho_s}) \\ \frac{1}{1-\phi_s}\Delta c(w_s - w_g\frac{\rho_g}{\rho_s}) \\ \frac{1}{1-\phi_s}\Delta c(E_s - E_g\frac{\rho_g}{\rho_s}) \\ -\Delta c \\ -\Delta c u_s \\ -\Delta c v_s \\ -\Delta c w_s \\ -\Delta c E_s \\ 0 \end{bmatrix}, S_2 = \begin{bmatrix} 0 \\ 0 \\ \frac{1}{1-\phi_s}(\frac{\Delta c}{2}-\delta)(u_g - u_s) \\ \frac{1}{1-\phi_s}(\frac{\Delta c}{2}-\delta)(v_g - v_s) \\ \frac{1}{1-\phi_s}(\frac{\Delta c}{2}-\delta)(w_g - w_s) \\ \frac{1}{1-\phi_s}(\frac{\Delta c}{2}-\delta)(U_g - U_s)U_s \\ 0 \\ -(\frac{\Delta c}{2}-\delta)(u_g - u_s) \\ -(\frac{\Delta c}{2}-\delta)(v_g - v_s) \\ -(\frac{\Delta c}{2}-\delta)(w_g - w_s) \\ -(\frac{\Delta c}{2}-\delta)(U_g - U_s)U_s \\ 0 \end{bmatrix}, S_3 = \begin{bmatrix} 0 \\ 0 \\ 0 \\ 0 \\ 0 \\ -\frac{1}{1-\phi_s}h(T_g - T_s) \\ 0 \\ 0 \\ 0 \\ 0 \\ h(T_g - T_s) \\ 0 \end{bmatrix} \quad (2)$$

where the three added source term vectors are related to the mass transfer (S_1), momentum (S_2), and energy (S_3) between the phases. The first row of the governing equations denotes chemical reaction handling k-th reactions. Second to 6th rows are the governing equations for gas-phase, and 7th to 12th rows are the governing equations for solid-phase. Subscript *g* denotes gas-phase, subscript *s* denotes solid-phase, and subscript *k* denotes *k*-th species respectively. ϕ_s denotes the solid-phase volume fraction, and N_p denotes particle number density. The terms U_g *and* U_s denote velocity vectors for gas and solid-phase. The terms T_g, T_s also denote the temperatures of the gas and solid respectively. The terms: δ, *d*, and *h* denote drag force factor, average particle diameter, and energy exchange factor between the phases respectively. They can be written as follows:

$$\delta = \frac{3}{4}(\phi_s / d)C_x \rho_g \left| u_g - u_s \right| \quad (3)$$

where C_x is the drag force coefficient obtained from a formula proposed by Hendrson[8].

$$d = (6\phi_s / \pi N_p)^{1/3} \quad (4)$$

$$h = 6\phi_s (Nu\lambda_g / d^2) \quad (5)$$

where Nu is a Nusselt number calculated from equations derived by Carlson and Hoglund[9].

$$Nu = \frac{2 + 0.459\,\mathrm{Re}^{0.55}\,\mathrm{Pr}^{0.33}}{1 + 3.42\dfrac{Ma}{\mathrm{Re}\,\mathrm{Pr}}(2 + 0.459\,\mathrm{Re}^{0.55}\,\mathrm{Pr}^{0.33})} \quad (6)$$

where Pr is the Prandtl number is defined as follows:

$$\mathrm{Pr} = \frac{C_{pg}\mu_g}{\lambda_g} \quad (7)$$

where C_{pg} is the gas-phase specific heats at constant pressure, μ_g is the gas-phase viscosity, and λ_g is thermal conductivity.

The interphase mass exchange factor Δc can be written as follows:

$$\Delta c = (3\phi_s\rho_s/\tau)(1 + 0.276\sqrt{\mathrm{Re}}) \quad \text{for T > T}_{\text{ignition}}\ (930\ \text{K}) \quad (8)$$

where Re is a relative Reynolds number based on the particle diameter and velocity difference between the gas and solid phase. τ is a characteristic time of combustion described as follows:

$$\tau = K_r d_0^2 \quad (9)$$

where *Kr* is a burning rate constant and d_0 is an initial diameter of particles.

We considered 4 reactions and 8 species [Al, Al_2O_3, AlO, O_2, H_2O, CO_2, H_2, C] in this study as follows:

$$Al + \frac{3}{4}O_2 = \frac{1}{2}Al_2O_3 - 810kJ/mol \quad \text{for T} \le \text{T}_{\text{decomposition}}\ (=3500\ \text{K}) \quad (10)$$

$$Al + \frac{1}{2}O_2 = AlO + 66.9kJ/mol \quad \text{for T > T}_{\text{decomposition}}\ (=3500\ \text{K}) \quad (11)$$

$$Al + \frac{3}{2}H_2O = \frac{1}{2}Al_2O_3 + \frac{3}{2}H_2 - 447.5kJ/mol \quad (12)$$

$$Al + \frac{3}{2}CO_2 = \frac{1}{2}Al_2O_3 + \frac{3}{2}C - 514.9kJ/mol \quad (13)$$

1-D COMPUTATIONS

Al-O_2 Detonation

To test the numerical model, an Al-O_2 detonation computation was performed. In this test case, detonation propagation in a dilute mixture of 5μm aluminum particles that were uniformly dispersed in an atmosphere of pure oxygen was calculated. The solid phase concentration was 1.5e-3 g/cc. The burning rate constant *Kr* was set to 4.0e6 s/m^2. The mesh resolution was 2 mm/cell. The other initial conditions were shown in Table 1.

Table 1: Initial conditions for Al-O2 detonation computation

	High pressure zone	Low pressure zone
Pressure	100 atm	1 atm
Gas phase temperature	2000 K	300 K
Gas-phase velocity	0 m/s	0 m/s
Solid-phase temperature	2000 K	300 K
Solid-phase velocity	0 m/s	0 m/s

Figure 1 shows the calculated pressure profiles of Al-O_2 detonation wave, while Fig. 2 shows the corresponding detonation velocity. The detonation velocity is unstable because the combustion (reaction) region separates and catches up with the shock front repeatedly during the propagation. The Chapman-Jouguet (C-J) detonation pressure obtained using Cheetah is about 37.1 atm and the C-J detonation velocity is about 164600 cm/s. The experimental pressure and detonation velocity published by Strauss [10] are about 32 atm and 155000-160000 cm/s correspondingly. The calculated pressure behind the peak (von-Neumann spike) is about 36 atm as shown in Fig. 1. The calculated detonation velocity is 152000 to 165000 cm/s. These calculated detonation pressure and velocity agree well with the C-J values and the experimental data.

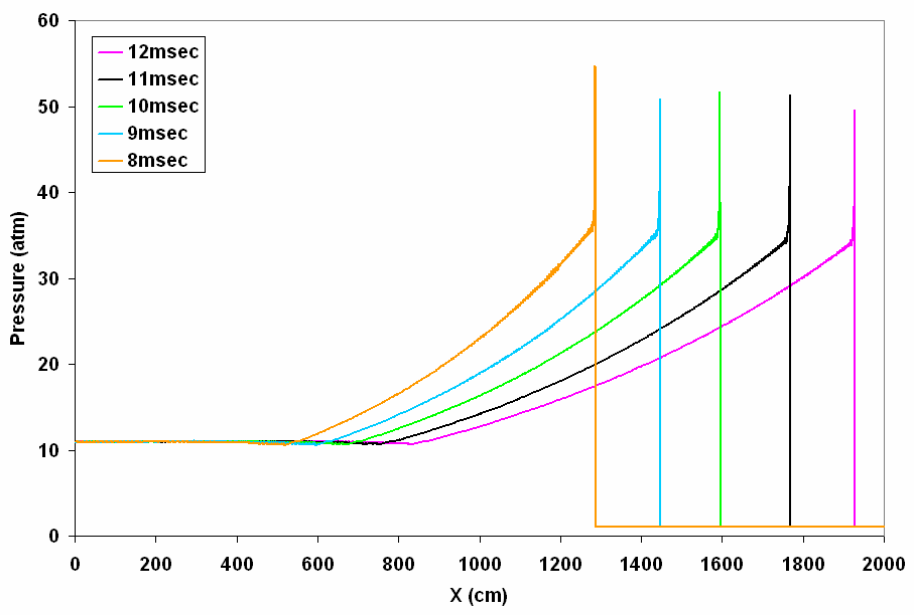

Fig. 1 Pressure profile of Al-O_2 detonation

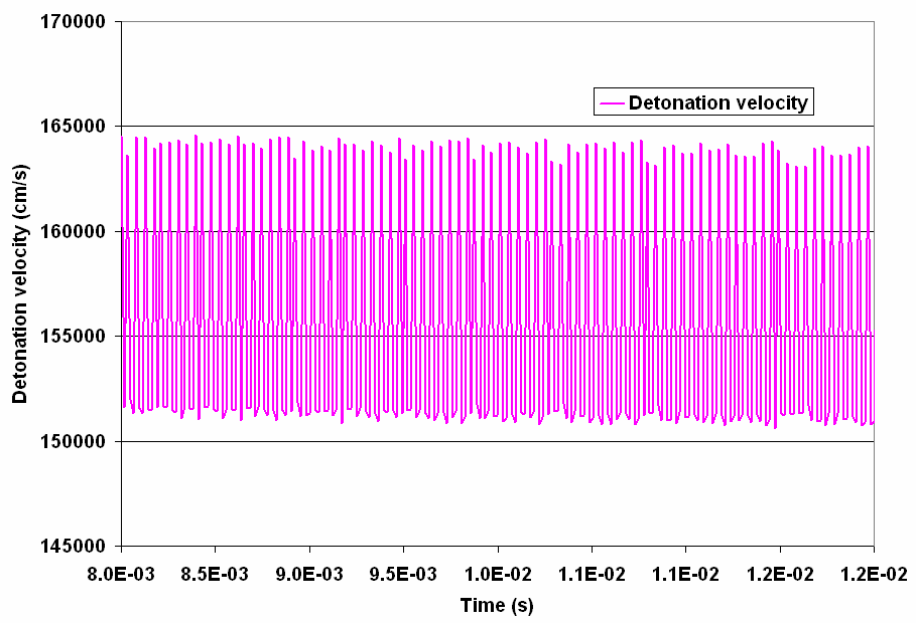

Fig. 2 Detonation velocity histories

Highly Aluminized HE Detonation Modeling

Here we modeled a stick of highly aluminized explosive with a length of 6cm. The JWL EOS [11] was used for detonation modeling from ignition to end of detonation. Cheetah was used to determine the initial detonation product species. Assuming the Aluminum particles were inert, Cheetah calculated the species fractions at frozen temperature (1800 K) as follows:

Table 2: Species fractions at frozen temperature (1800 K)

Name	Phase	(mol/kg)	(mol gas/mol HE)
h2o	Gas	7.72E+00	4.55E-01
n2	Gas	4.38E+00	2.59E-01
co2	Gas	4.09E+00	2.41E-01
hcl	Gas	2.55E+00	1.51E-01
ch4	Gas	2.24E+00	1.32E-01
co	Gas	1.72E+00	1.02E-01
nh3	Gas	5.23E-01	3.08E-02
h2	Gas	3.55E-01	2.09E-02
other gas products	Gas	3.22E-01	1.83E-02
liquid products	Liquid	1.22E+01	7.22E-01
solid products	solid	2.61E+00	1.54E-01

Total Gas	2.39E+01	1.41E+00
Total Cond.	1.48E+01	8.76E-01

From this Cheetah results, the 8 species used in Eqns. (10) - (13) were chosen as initial detonation products. The JWL parameters were also obtained from Cheetah calculation.

Reaction Model Effects

Figure 3 shows pressure profiles at 0.15 msec for three cases where different reactions are considered. The Al particle diameter is set to 5μm. The black line (Al_inert) denotes the pressure profile where aluminum particles were inert. The green line (one-reaction_Al5micron) denotes the case where aluminum particles were only reacted with oxygen as per Eq. (10). The magenta line (Four-reactions_Al5micron) denotes the case where all reactions in Eqns. (10) to (13) were considered. The reaction in Eq. (12) and (13) release less energy than the energy released in Eq. (10) as the reaction in Eq. (11) is endothermic. Hence the pressure for the case modeling all four reactions (Eqns. (10) to (13)) is less than that for the case considering only one reaction in Eq. (10).

Figure 4 shows the species density profiles at 0.15 msec when all reactions were considered. The Al particles around the surface of the HE were reacted with Oxygen in the ambient region and AlO was generated. The small amount of generated AlO was located close to the blast wave front region. On the other hand, most of the Al particles were reacted with H_2O and CO_2 in the detonation products and Al_2O_3 was formed. Hence, most of the Al_2O_3 existed behind the blast wave front. The amount of AlO is significantly smaller than other species. Hence AlO density is plotted separately in Fig. 4.

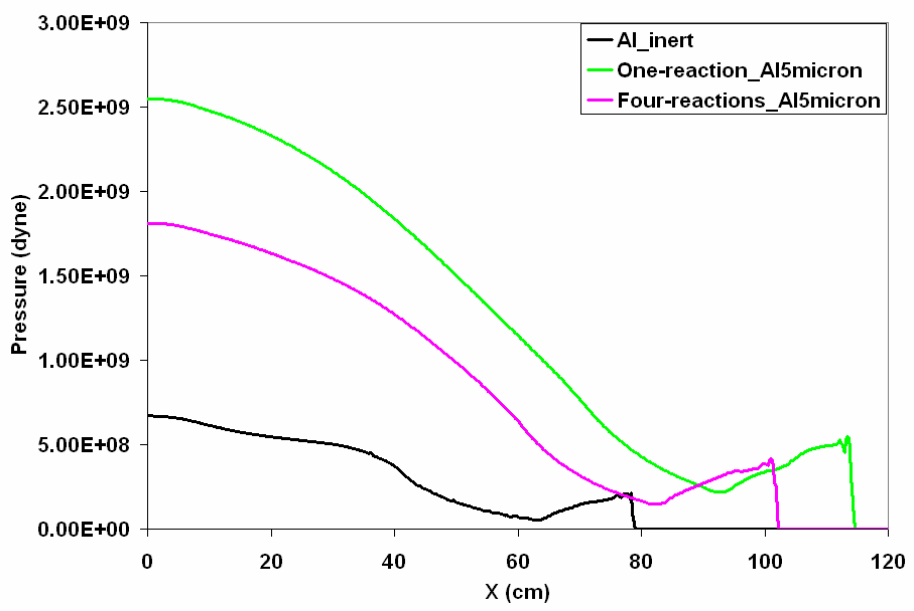

Fig. 3 Pressure profiles at 0.15 msec. 1-D Al burning behind the blast wave

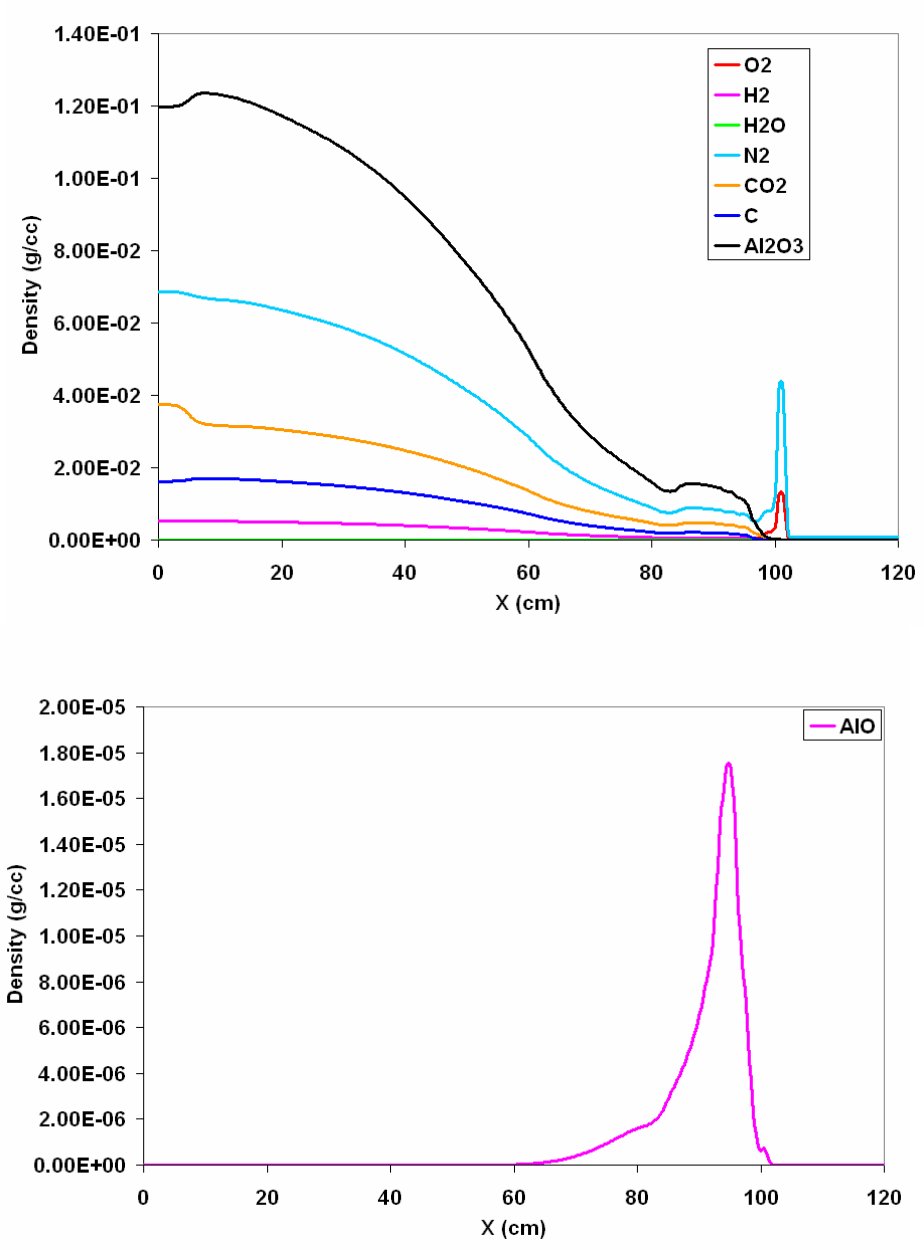

Fig. 4 Species densities at 0.15 msec 1-D Al burning behind the blast wave

Particle Diameter Effect

Figures 5, 6, and 7 show pressure, impulse, and Al solid phase concentration profiles at 0.15 msec for explosives that contained different particle diameter sizes. All reactions in Eqns. (10) – (13) are considered for this test. The black, magenta, and green lines in Figs. 5-7 show the results for 5μm, 50μm 500μm diameters respectively. The light blue line in Fig. 7 shows the Al solid phase concentration initial value. The 5μm Al particles burned quickly and produced the highest pressure values at 0.15 msec as shown in Fig. 5. On the other hand, the 500μm Al particles did not burn completely and resulted in the lowest pressure values. Figure 8 shows pressure and impulse comparison among the different particle diameter cases when the blast front reached 100

cm from ignition point. The difference of evaporating and burning velocity caused the different pressure and impulse profiles shown here. Tables 3 and 4 show the pressure and impulse values at ignition point (X = 0). The 5μm particles burned quickly and resulted in the highest pressure and impulse value at this location. Since the 50μm particles and 500μm particles burned slower as they propagated behind the blast wave, they released energy farther downstream. The pressure value of 50μm case at ignition point is higher than that of 5μm case at this time because the Al particles are still burning, as shown in Figs. 6 and 7. Never the less, table 4 shows that as all wave propagated a distance of 100cm, the complete release of energy from the 5μm particles yields higher pressure and impulse than the still burning 50μm particles, which, in turn is higher than the slower burning 500μm particles.

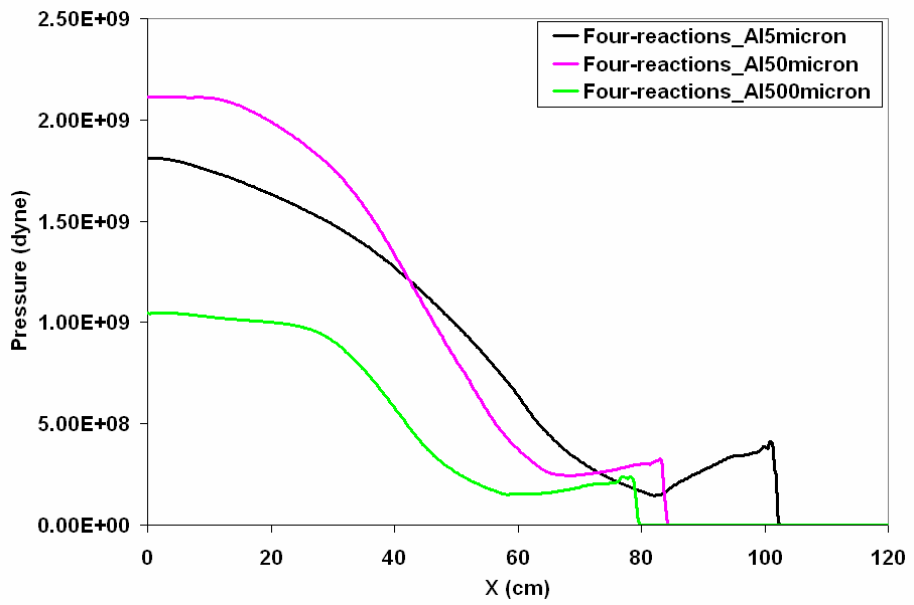

Fig.5 Pressure profiles at 0.15 msec for 3 different particle diameters (5, 50, and 500μm)

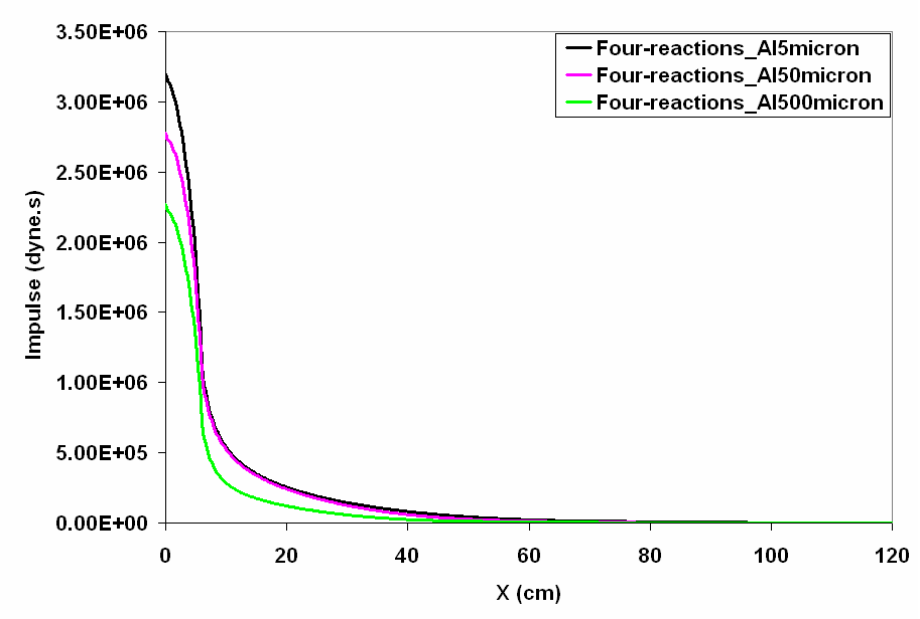

Fig.6 Impulse profiles at 0.15 msec for 3 different particle diameters (5, 50, and 500μm)

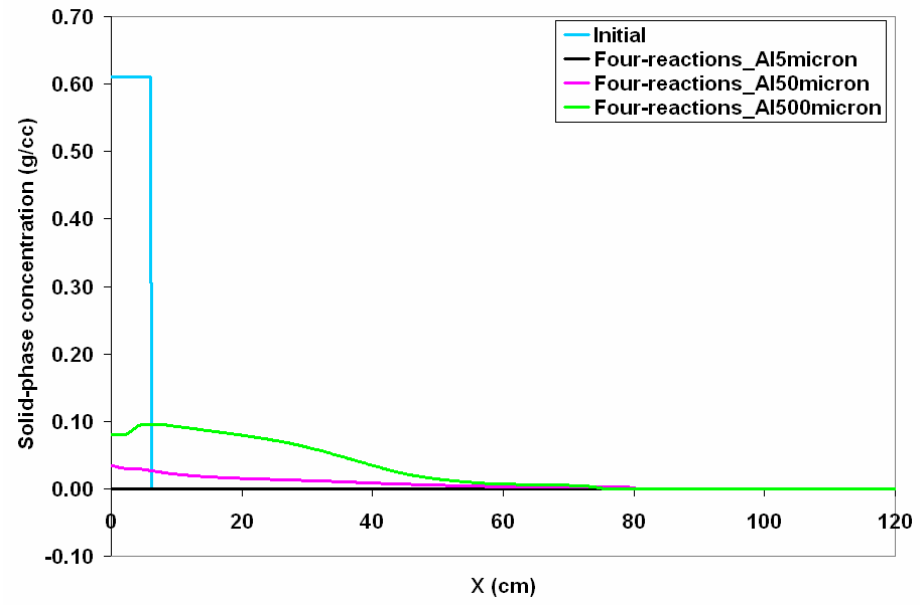

Fig.7 Aluminum solid phase concentration profiles at 0.15 msec for 3 different particle diameters (5, 50, and 500μm)

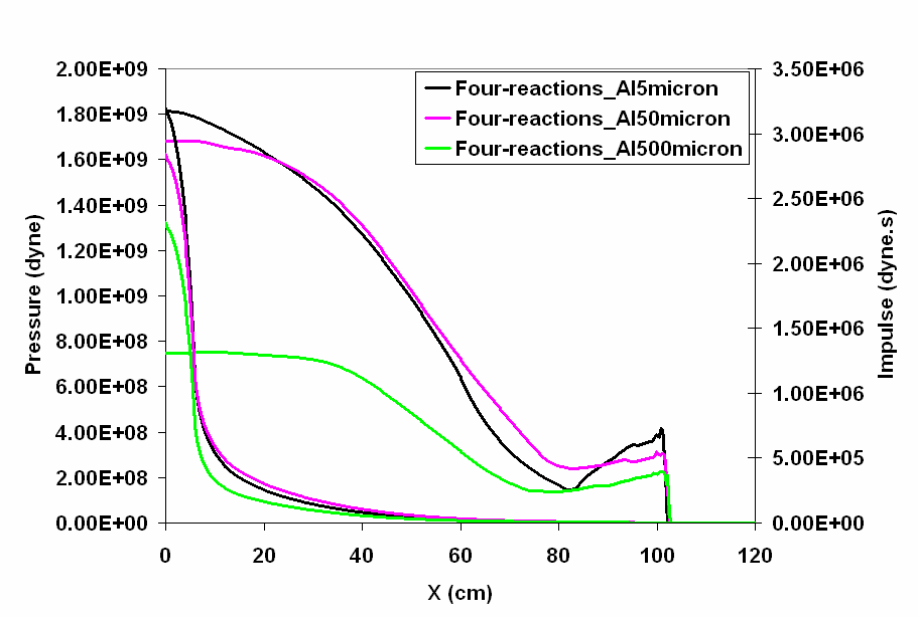

Fig. 8 Pressure and Impulse profiles when the blast front reached 100cm from the ignition point for 3 different particle diameters (5, 50, and 500μm)

Table 3. Pressure and Impulse value at ignition point at 0.15 msec for 3 different particle diameters (5, 50, and 500μm)

Time = 0.15 msec	Pressure (dyne)	Impulse (dyne.s)
5μm particles	1.81e9	3.20e6
50μm particles	2.11e9	2.77e6
500μm particles	1.05e9	2.27e6

Table 4. Pressure and Impulse value at ignition point when the blast front reached 100cm from the ignition point for 3 different particle diameters (5, 50, and 500μm)

Blast front location = 100cm	Pressure (dyne)	Impulse (dyne.s)
5μm particles	1.81e9	3.20e6
50μm particles	1.68e9	2.84e6
500μm particles	7.46e8	2.31e6

3-D COMPUTATIONS

The aluminum burning model, which was tested in 1-D code, was incorporated into our in-house 3D code, FEFLO. Figure 9 shows the pressure Gouraud shading of the small tube test. The HE

modeled here is 6 cm thick with average 5μm Al particle diameters. Figure 10 shows the comparison of pressure profiles between results obtained with and without the aluminum burning.

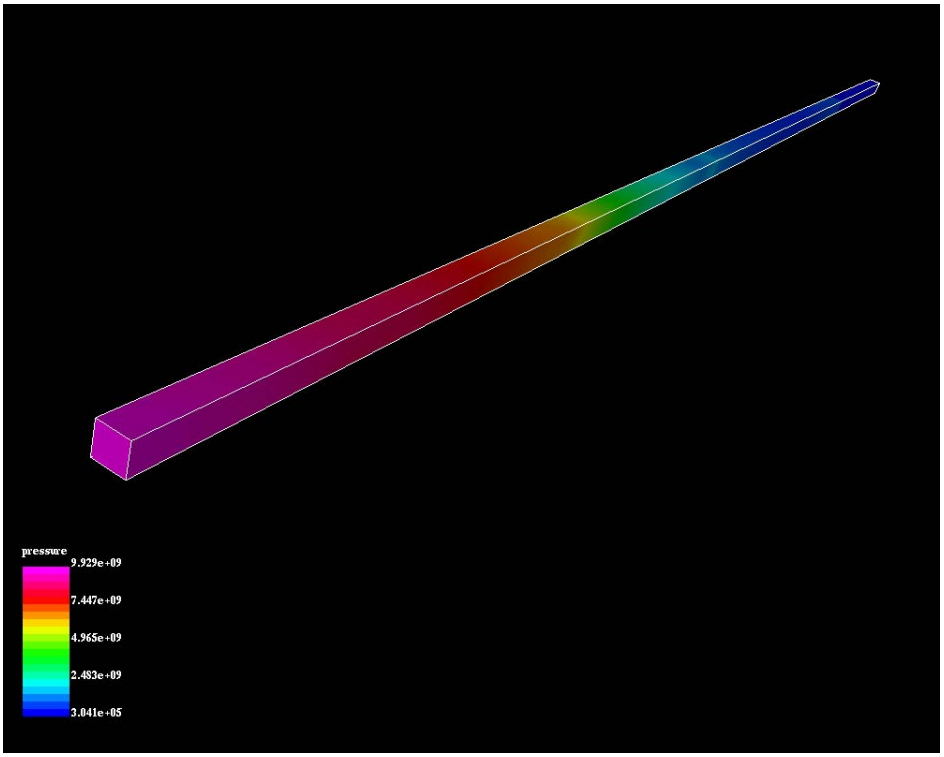

Fig. 9 Pressure Gouraud shading at 50 μsec

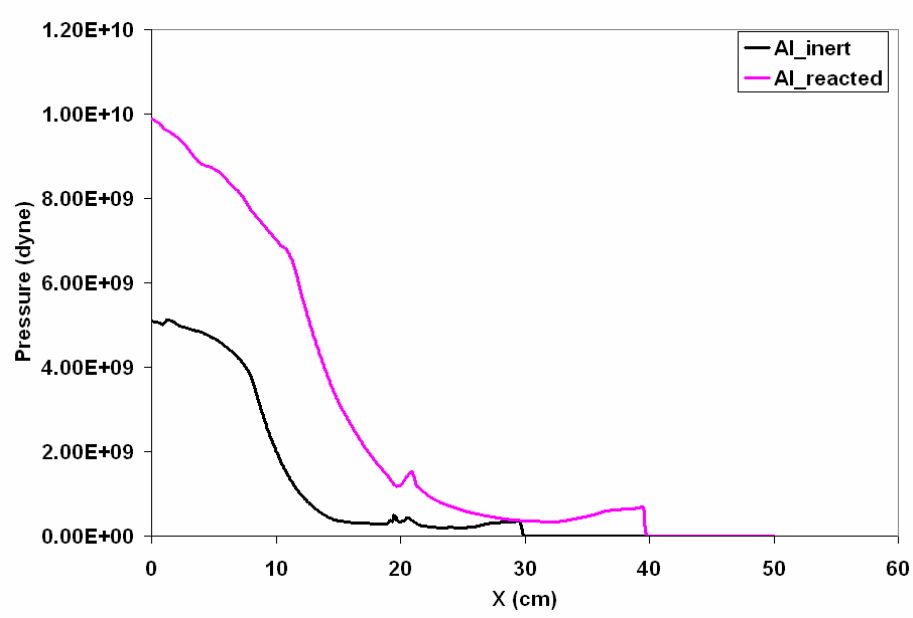

Fig. 10 Pressure profiles at 50 μsec. (magenta: with Al particles, Black: Inert Al particles)

CONCLUDING REMARKS

Energy release by aluminum burning behind the blast wave of heavily aluminized explosives was investigated. An aluminum evaporation/reaction model within the multi-phase flow was applied. The applied model was validated via 1-D Al-O_2 detonation wave computation. The computed values are agreed well with C-J values.

As a first step in the overall 3-D comprehensive methodology development, the evaporation of small aluminum particles, with 5, 50, and 500μm diameter, was investigated in a 1-D code. The aluminum particles can react with oxygen, water, and carbon dioxide. The modeled HE includes a significant percentage of aluminum particles, whose long-time afterburning and energy release must be considered.

The resulting pressure profiles are different from those obtained for the no-reaction case or using a one-reaction which only consider the reaction with oxygen. The Al particle size difference also shows the different pressure profiles. While the 5μm particles were burned immediately behind the blast wave, the 50/500μm particles were burned slower behind the blast wave.

Finally the aluminum burning model was incorporated into our in-house 3-D code, FEFLO. In the final presentation, more 3-D computed results will be presented.

REFERENCES

[1] C.K. Kim, J.G. Moon, J.S. Hwang, M.C. Lai, and K.S. Im, “Afterburning of TNT Explosive Products in Air with Aluminum Particles,” AIAA-2008-1029, 2008

[2] K. Balakrishnan and S. Menon, “On the Role of Ambient Reactive Particles in the Mixing and Afterburn Behind Explosive Blast Waves,” *Combust. Sci. and Tech.*, vol 182, pp.186-214, 2010

[3] A. Khasainov, B. Veyssiere, “Steady, Plane, Double-front Detonations in Gaseous Detonable Mixtures Containing a Suspension of Aluminum Particles,” *Dynamics of Explosions: Progress in Astronautics and Aeronautics* 114, AIAA, pp284-299, 1988.

[4] A. L. Kuhl, R.E. Ferguson, and A.K. Oppenheim, “Gas dynamic model of turbulent exothermic fields in explosions,” *Progress in Astronautics and Aeronautics Series*, 173, pp. 251-261, 1997

[5] D. Schwer and K. Kailasanath, “Blast Mitigation by Water Mist (1) Simulation of Confined Blast Waves,” NRL/MR/6410-02-8636.

[6] I. A. Johnston, “The Noble-Abel equation of state: Thermodynamic derivations for ballistics modeling. *Defense Sci. Tech. Org*., DSTO-TN-0670, 2005

[7] Paul W. Cooper, and Stanley R. Kurowski, “Introduction to the Technology of Explosives,” WILEY-VCH.

[8] C.B. Henderson, “Drag Coefficients of Spheres in Continuum and Rarefied Flows,” *AIAA J.* vol. 14, No. 6, pp. 707-708, 1976

[9] D.J. Carlson and R.F. Hoglund, “Particle Drag and Heat Transfer in Rocket Nozzles,” *AIAA J*. vol.14, No. 11, pp.1980-1984, 1964

[10] W. A. Strauss, “Investigation of the Detonation of Aluminum Powder-Oxygen Mixtures,” *AIAA J*. vol. 6, No. 9, pp.1753-1756, 1968

[11] P.C. Souers, Ben Wu, and L.C. Haselman, Jr., “Detonation Equation of State at LLNL, 1995,” Energetic Materials Center Lawrence Livermore National Laboratory, February 1, 1996